

Latent Linear Quadratic Regulator for Robotic Control Tasks

Yuan Zhang

University of Freiburg, Germany
yzhang@cs.uni-freiburg.de

Shaohui Yang

EPFL, Switzerland
shaohui.yang@epfl.ch

Toshiyuki Ohtsuka

Kyoto University, Japan
ohtsuka@i.kyoto-u.ac.jp

Colin Jones

EPFL, Switzerland
colin.jones@epfl.ch

Joschka Boedecker

University of Freiburg, Germany
jboedeck@informatik.uni-freiburg.de

Abstract: Model predictive control (MPC) has played a more crucial role in various robotic control tasks, but its high computational requirements are concerning, especially for nonlinear dynamical models. This paper presents a **latent linear quadratic regulator (LaLQR)** that maps the state space into a latent space, on which the dynamical model is linear and the cost function is quadratic, allowing the efficient application of LQR. We jointly learn this alternative system by imitating the original MPC. Experiments show LaLQR’s superior efficiency and generalization compared to other baselines.

Keywords: Model predictive control, Linear quadratic regulator, Imitation learning, Lifting, Embedding, Robotics

1 Introduction

Model predictive control (MPC) has been widely studied in the field of robotic control, e.g. quadruped locomotion [1, 2] and drone racing [3]. As a model-based method, MPC strongly relies on an effective discrete-time dynamical model of the system, $x_{h+1} = f(x_h, u_h)$, where x, u represent state and control respectively. Model accuracy enables MPC with future prediction and optimization of control actions to be taken. However, solving an instance of MPC problem can be extremely computationally expensive [4], especially for nonlinear dynamical model f , making it limited for online deployment on embedded devices.

To solve an MPC problem with a generic nonlinear dynamical model, a sequential quadratic programming (SQP) [5] approach is frequently leveraged. SQP forms and solves quadratic programming (QP) iteratively. Each QP is composed of linearization of the dynamics $\delta x_{h+1} = \frac{\partial f}{\partial x} \delta x_h + \frac{\partial f}{\partial u} \delta u_h$ up to 1st order, constraints up to 1st order, and cost function up to 2nd order. Another more efficient approach is the localized linear quadratic regulator (LoLQR) [6], which linearizes the dynamical model at the target point with Taylor expansion and adopts linear quadratic regulator (LQR) [7]. However, such local approximation easily explodes for predictions in other locations far from the equilibrium. Recently, another line of approaches, imitation learning (IL), has become popular in comply with the development of machine learning [8]. It is able to fit complex mappings from state x_h to control u_h perfectly with a neural network (NN) provided sufficient data and model capacity. Naturally, IL inherits the deficits of learning-based methods, such as poor generalization in unseen scenarios not covered by the training dataset.

In this paper, we propose a **latent linear quadratic regulator (LaLQR)** approach and strive to overcome the aforementioned drawbacks. In specific, the original state x_h is transformed to a latent state z_h with a nonlinear mapping function ϕ (represented as a NN in practice). The mapping is further regularized with linear dynamics and quadratic costs on the latent space. Therefore, the classic LQR can be performed on this latent space. It utilizes the efficiency of LQR and simultaneously maintains

the accuracy with the global nonlinear mapping function. Compared with the other learning-based method IL, LaLQR indicates greater generalization ability in the experiments. The comparison of all methods is summarized in Table 1.

Table 1: Comparison of some popular control methods for nonlinear systems.

Method	dynamical model	Optimizer	Accuracy	Efficiency	Generalization
SQP	nonlinear	SQP	+	-	+
LoLQR	linear	LQR	-	+	-
IL	-	NN	+	+	-
LaLQR	latent linear	NN + LQR	+	+	+

2 Background

2.1 Model Predictive Control

Model predictive control (MPC) solves a finite horizon optimal control problem parametrized by the current state $x(t)$, generates an optimal control sequence, applies the first element only, and re-plans with the new state measurement. In general, a discrete-time MPC consists of a dynamical model $x_{h+1} = f(x_h, u_h)$, a stagewise cost function $c(x_h, u_h)$, and an optimization algorithm finding the optimal $\{u_0^*, u_1^*, \dots, u_H^*\}$. The mathematical formulation of the optimization problem is as follows:

$$\begin{aligned} \min_{u_0, u_1, \dots, u_H} \quad & \sum_{h=0}^H c(x_h, u_h) \\ \text{s.t.} \quad & x_{h+1} = f(x_h, u_h) \quad x_0 = x(t). \end{aligned} \quad (1)$$

2.2 Linear Predictors for Nonlinear Controlled Systems via Koopman

Lifting the state space to a higher dimension plays a key role in obtaining predictions of a nonlinear dynamical system $x^+ = f(x, u)$ as the output of a linear one. For uncontrolled dynamical systems, this idea can be justified with the Koopman operator theory. For controlled systems, the justification requires the extension of state space, the new definition of observables and their residing Hilbert space. In this paper, we follow a both rigorous and practical way of generalizing the Koopman operator \mathcal{K} to controlled systems as in [9]¹:

$$\mathcal{K} \begin{bmatrix} \phi(x) \\ \mathbf{u}(0) \end{bmatrix} = \begin{bmatrix} \phi(f(x, \mathbf{u}(0))) \\ (\mathcal{S}\mathbf{u})(0) \end{bmatrix} = \begin{bmatrix} \phi(f(x, \mathbf{u}(0))) \\ \mathbf{u}(1) \end{bmatrix}, \mathbf{u}(0) = u. \quad (2)$$

This leads to the following (approximate) linear evolution in the lifted state space $z = \phi(x) \in \mathbb{R}^N$ while the control space remains unchanged: $z^+ = \phi(x^+) = A\phi(x) + B\mathbf{u}(0) = Az + Bu$.

3 Latent Linear Model Predictive Control

It is well known that nonlinear MPC suffers from a high computational burden and is thus hard to deploy on embedded devices. This paper tackles this problem by transforming the nonlinear MPC formulation into a latent linear one and adopting a linear quadratic regulator (LQR) to acquire the optimal control inputs. We learn the parameters of the new formulation by imitating the original nonlinear MPC. In the end, we analyze the stability of to validate the proposed structure.

¹ $\mathbf{u} = \{u_i\}_{i=0}^\infty$ denotes the control sequence till infinity, \mathcal{S} is the left shift operator.

3.1 Latent Linear Quadratic Problem

The dynamical model $x_{h+1} = f(x_h, u_h)$ is nonlinear in general cases, with state $x_h \in \mathbb{R}^n$ and control $u_h \in \mathbb{R}^m$. Based on the Koopman operator introduced in Section 2.2, the nonlinear system can be lifted to an (approximately) equivalent linear system, leveraging a finite-dimensional transformation. The state x_h is mapped to the latent state $z_h \in \mathbb{R}^N$, $N > n$ with the embedding function $z_h = \phi(x_h)$. On the latent space, the dynamical model becomes linear: $z_{h+1} = Az_h + Bu_h$, where $A \in \mathbb{R}^{N \times N}$ and $B \in \mathbb{R}^{N \times m}$ are matrices with learnable parameters. We visualize these two types of dynamical models in Figure 1 for clear comparison.

Beyond the dynamical model, a cost function on the latent space shall be constructed as in Equation 1. Ideally, a quadratic cost $z_h^T Q z_h + u_h^T R u_h$ with positive semi-definite matrices $Q \in \mathcal{S}_+^N$ and $R \in \mathcal{S}_+^m$ is preferred for ease of computation. However, finding the direct bijection for any cost functions $c(x_h, u_h)$ is difficult. Instead, we include an additional trainable monotonic function $F : \mathbb{R} \rightarrow \mathbb{R}$ to bridge two costs $c(x_h, u_h) = F(z_h^T Q z_h + u_h^T R u_h)$. Combining both the dynamical model and the cost function, we achieve the new latent linear quadratic problem and its connection to the nonlinear MPC as follows:

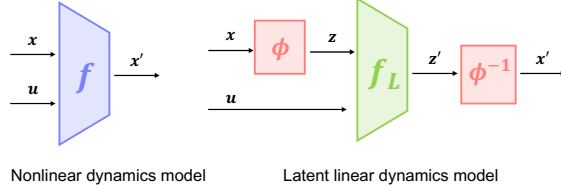


Figure 1: Visualization of two types of dynamical models. f_L means the linear dynamical model.

$$\begin{aligned} \text{Equation 1} \implies & \min_{u_0, u_1, \dots, u_H} \sum_{h=0}^H z_h^T Q z_h + u_h^T R u_h \\ \text{s.t.} \quad & z_{h+1} = Az_h + Bu_h \quad x_0 = x(t) \\ & z_h = \phi(x_h) \quad F(z_h^T Q z_h + u_h^T R u_h) = c(x_h, z_h). \end{aligned} \quad (3)$$

We further discuss the practical designs of the different modules in the latent linear MPC formulation and rationalize our choices.

Embedding Function The embedding function ϕ is dimension-raising since N is set larger than n according to the Koopman theory. It is implemented as a feed-forward neural network. Notably, it doesn't have to be reversible as we don't need to reconstruct the next state x' to make plans. All optimization is carried out on the latent space z .

Linear dynamical model Leaving sufficient degrees of freedom to the lifting function ϕ , we fix the shape of the linear system (A, B) apriori, to be controllable companion form [10] in the latent space. Specifically, for systems with N states and m inputs, the structure of A and B is uniquely defined by the controllability (Kronecker) indices $\{\mu_i\}_{i=1}^m$:

$$\begin{aligned} A = [A_{ij}] \quad A_{ii} &= \begin{bmatrix} 0 & & \\ \vdots & \mathbf{I}_{\mu_i-1} & \\ 0 & \diamond \dots \diamond \end{bmatrix} \in \mathbb{R}^{\mu_i \times \mu_i} \quad A_{ij} = \begin{bmatrix} 0 & \dots & 0 \\ \vdots & & \vdots \\ 0 & \dots & 0 \\ \diamond & \dots & \diamond \end{bmatrix} \in \mathbb{R}^{\mu_i \times \mu_j} \quad i \neq j \\ B = \begin{bmatrix} B_1 \\ \vdots \\ B_m \end{bmatrix} \quad B_i &= \begin{bmatrix} \mathbf{0}_{(\mu_i-1) \times (m-i)} \\ \mathbf{0}_{\mu_i \times i} & 1 \diamond \dots \diamond \end{bmatrix} \in \mathbb{R}^{\mu_i \times m}, \end{aligned} \quad (4)$$

where \mathbf{I}_j denotes identity matrix of size $j \times j$, $\mathbf{0}_{j \times k}$ denotes zero matrix of size $j \times k$, and \diamond represents the learnable parameters in the matrix. Notably, all parameters are initialized from zero to ensure full

controllability. The Kronecker indices are empirically set to be constant across stages $\mu_i = \lfloor N/m \rfloor$. The companion form owns the advantage of the least learnable parameters for controllable (A, B) , of size $Nm + m(m-1)/2$, compared with the general case of $N^2 + Nm$. There is another line of work [11, 12] using the diagonal structure in the matrix A for fewer parameters, but they are either complex values or uncontrollable on the latent space. We will analyze the differences from other structures theoretically and empirically in the following sections.

Quadratic Cost Function $Q \in \mathcal{S}_+^N, R \in \mathcal{S}_+^m$ are positive semi-definite matrices for reasonable control performances. To achieve this, we introduce two auxiliary matrices $\hat{Q} \in \mathbb{R}^{N \times N}, \hat{R} \in \mathbb{R}^{m \times m}$ and construct $Q = \mathbf{I}_N + \hat{Q}\hat{Q}^T, R = \mathbf{I}_m + \hat{R}\hat{R}^T$. Regarding the monotonic function F , we adopt the Lipschitz monotonic networks (LMN) [13], which is efficient and compatible with the backpropagation calculation.

3.2 Linear Quadratic Regulator on Latent Space

Thanks to the transformation from the raw state x into the latent state z in the last section, we now have an optimal control problem with the linear dynamical model (A, B) and the quadratic cost function (Q, R) as Equation 3, making the use of linear quadratic regulator [7] (LQR) possible. We then extend the horizon from H to ∞ for practical reasons: (1) the practical value H in MPC is usually large enough and its solution is equivalent to the infinite horizon; (2) it is easy to design an efficient control law with infinite horizon. Afterwards, we can calculate a static gain matrix $K \in \mathbb{R}^{N \times m}$ based on the matrices A, B, Q, R , by solving the Riccati function. Since the matrix K can be pre-computed, the only online computation to execute optimal control at each step is $u_h = -Kz_h = -K\phi(x_h)$.

3.3 Learning System Parameters

With the reformulation process in Section 3.1, it is necessary to identify the parameters of the latent linear quadratic problem, including A, B, Q, R, F, ϕ . We concisely adopt only two objectives to automatically detect those parameters.

Consistency Loss The first objective is named consistency loss, which evaluates the latent linear dynamical models in two consecutive steps. In mathematics, for a transition tuple (x_h, u_h, x_{h+1}) satisfying the nonlinear dynamics $x_{h+1} = f(x_h, u_h)$, the consistency loss is expressed as $\mathcal{L}_{\text{consistency}}(x_h, u_h, x_{h+1}) = \|\phi(x_{h+1}) - (A\phi(x_h) + Bu_h)\|_2^2$. Tang et al. [14] used stop-gradient calculation on next latent state as $\text{sg}(\phi(x_{h+1}))$ to avoid the representation collapse in the learning process. In our method, sg is unnecessary due to the special companion structure and the following cost loss to regularize the latent space.

Cost Loss The second objective focuses on the predictions on the cost function. For the cost $c_h = c(x_h, u_h)$ inside the original MPC problem, the cost loss is denoted as $\mathcal{L}_{\text{cost}}(x_h, u_h, c_h) = \|c_h - F(\phi(x_h)^T Q \phi(x_h) + u_h^T R u_h)\|_2^2$.

By combining these two loss functions, we can derive a practical algorithm to imitate the original nonlinear MPC to a latent linear quadratic problem and calculate the control law for online usage. The detailed algorithm is described in Appendix A. One may compare our proposed method to the normal imitation learning methods, which directly learn a policy function $u_h = \pi(x_h)$ by imitating the control signals generated by the nonlinear MPC. In comparison, we imitate the entire MPC problem instead of only the closed-loop control. It offers a benefit to possibly produce optimal control performances even with sub-optimal nonlinear MPC controllers, while the imitation learning methods are restricted by the targets they learn from. We further empirically compare the generalization of these two methods in Section 4.3.

3.4 Stability Analysis

In this section, we analyze the stability of the learned latent linear quadratic system, to prove the validity of our proposed method. Denote the stable state and control of the system as x_T, u_T . We

can linearize the nonlinear dynamical system with the first-order Taylor expansion at the stable point as $\delta x_{h+1} = \frac{\partial f}{\partial x}|_{x=x_T} \delta x_h + \frac{\partial f}{\partial u}|_{u=u_T} \delta u_h$. Suppose there exists a state feedback control law $\delta u_h = L\delta x_h$, an autonomous system is derived as $\delta x_{h+1} = (\frac{\partial f}{\partial x}|_{x=x_T} + \frac{\partial f}{\partial u}|_{u=u_T} L)\delta x_h = C\delta x_h$.

Compared with our proposed method, the latent dynamical model is written as $\phi(x_{h+1}) = A\phi(x_h) + Bu_h$ and whose derivative goes with $\frac{\partial \phi}{\partial x}|_{x=x_T} \delta x_{h+1} = A\frac{\partial \phi}{\partial x}|_{x=x_T} \delta x_h + B\delta u_h$. The control law $u_h = -K\phi(x_h)$ is calculated as introduced in Section 3.2, and its derivative $\delta u_h = -K\frac{\partial \phi}{\partial x}|_{x=x_T} \delta x_h$. The corresponding autonomous system is thus written as $\frac{\partial \phi}{\partial x}|_{x=x_T} \delta x_{h+1} = (A - BK)\frac{\partial \phi}{\partial x}|_{x=x_T} \delta x_h = D\frac{\partial \phi}{\partial x}|_{x=x_T} \delta x_h$. Regarding the two equivalent systems at the stable point, the following proposition holds.

Proposition 1 (Eigenvalues and eigenvectors of equivalent systems) *The local linear autonomous system $\delta x_{h+1} = C\delta x_h$ and the latent linear autonomous system $\frac{\partial \phi}{\partial x}|_{x=x_T} \delta x_{h+1} = D\frac{\partial \phi}{\partial x}|_{x=x_T} \delta x_h$ are equivalent at the stable point x_T if and only if for any matrix C 's eigenvalue λ and its corresponding eigenvector v , λ and $\frac{\partial \phi}{\partial x}|_{x=x_T} v$ are also the eigenvector and eigenvalue of the matrix D .*

In practice, we can testify the value of the eigen loss close to 0, denoted as $\mathcal{L}_{\text{eigen}} = \sum_{i=1}^n \|D\frac{\partial \phi}{\partial x}|_{x=x_T} v_i - \lambda_i \frac{\partial \phi}{\partial x}|_{x=x_T} v_i\|_2$, where λ_i, v_i are eigenvalue and eigenvector pair of the matrix C . We plot the curve of this value during training in the experiment of *cartpole* (the specific environmental setup will be introduced in Section 4.1). As is shown in Figure 2, the loss of the companion format continuously decreases as the training progresses, showing that it is approaching the original nonlinear system at the stable point. "full" means the full matrix A are learnable. Its eigen loss also declines but in a more unstable manner, resulting from the large parameter space during training. The diagonal A can't satisfy such relations. With only real-valued parameters used in the diagonal position, it doesn't have enough representational ability for the original system. The previous work [12] suggested using the complex-valued diagonal representation but was rather difficult to combine with other modules in our case.

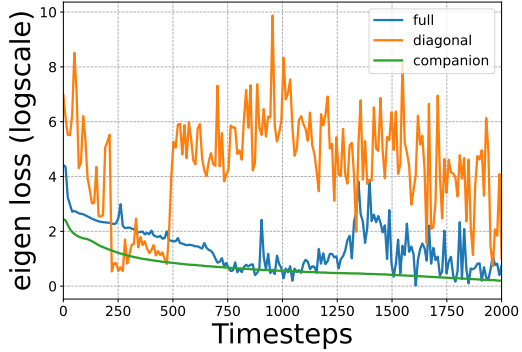


Figure 2: Training curve of eigen loss on *cartpole* task. The x-axis is the training time steps and the y-axis is the average eigen loss (in log scale) during training.

4 Experiments

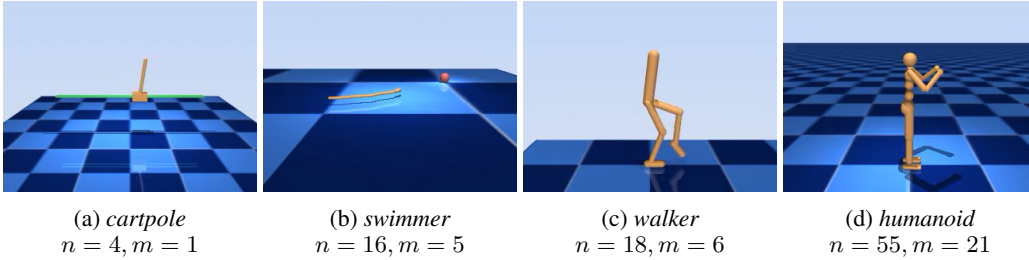


Figure 3: Visualization of robots used in the experiments, with increased complexity.

4.1 Experimental Setup

Task Setup We utilize MuJoCo [15] as the simulated platform to evaluate all baselines. Based on that, we select 4 robots *cartpole*, *swimmer*, *walker* and *humanoid*, with increased complexity in state and action spaces as illustrated in Figure 3. For *cartpole*, the controller needs to balance the pole in the origin position. For *swimmer*, the robot is driven to reach the target position (as drawn in red ball). For *walker* and *humanoid*, the controller needs to balance the robot at a certain height. The specific introduction of these tasks can be referred to Appendix B. We evaluate each controller by running it 100 times and reporting the total costs over the trajectory and the average computational time (in milliseconds) for each planning step.

Baselines We compare our methods against the following baselines.

- **SQP** adopts the full nonlinear dynamical model of $x_{h+1} = f(x_h, u_h)$ and ground truth cost function $c(x_h, u_h)$, and further utilizes iLQG [16] as the planner to generate optimal control. The method is essentially a Gauss-Newton method utilizing first- and second-order derivative information and thus is expensive to perform.

- **LoLQR** expands the nonlinear dynamical model at the stable point (x^*, u^*) with Taylor expansion, and uses this linear dynamics globally for efficient control. Notably, this method requires prior knowledge of the stable point.

- **IL** directly learns a control policy $u_h = \pi(x_h)$ by imitating the output of **SQP** with a neural network. The network structure is set as a feed-forward neural network with the same hidden units as the proposed method. The data used for training is the same as the one by our proposed method.

- **LaLQR (Ours)** represents the proposed method in Section 3. After imitation learning the nonlinear MPC as Algorithm 1, the control policy is set as $u_h = -K\phi(x_h)$ during testing online, which is the only computation required. The specific planning hyperparameters for SQP and LoLQR, and the training hyperparameters for IL and LaLQR can be found in Appendix B.2.

4.2 Main Results

For each robotic task, we train both IL and LaLQR controllers until convergence on the same dataset generated by the SQP controller. All models are well-fitted with losses under 0.05. The specific training curves are presented in Appendix C.1. The more appealing result is the testing performances as shown in Table 2. For control efficiency, both LaLQR and IL require much less computational time compared with the original SQP controller, since there is no complex optimization process but only simple forward matrix multiplication. All calculations are executed on the same CPU machine. With GPU, further acceleration can be achieved for IL and LaLQR. Of course, LoLQR is the fastest algorithm with linear dynamics on the original state space. However, its control performance is the worst due to its local dynamical model. LaLQR achieves competitive or excelling control results compared with IL for all tasks. Its total cost even approaches SQP for *cartpole* and *swimmer*.

Table 2: Testing results on 4 simulated robotic tasks. Total cost is the sum of step-wise cost over the testing trajectory and average time (in milliseconds) is the required time for each planning step. All reports are reported in average and standard deviation over 100 runs.

Tasks		SQP	LoLQR	IL	LaLQR (Ours)
<i>cartpole</i>	total_cost	3042.56 \pm 2156.08	3366.04 \pm 1911.97	3121.99 \pm 2115.25	3141.30 \pm 1815.42
	average_time	10.26 \pm 0.42	0.02 \pm 0.00	0.25 \pm 0.07	0.24 \pm 0.05
<i>swimmer</i>	total_cost	365.07 \pm 9.55	692.15 \pm 8.91	419.54 \pm 9.41	418.63 \pm 6.81
	average_time	43.88 \pm 2.90	0.03 \pm 0.01	0.34 \pm 0.10	0.32 \pm 0.09
<i>walker</i>	total_cost	2.92 \pm 0.03	130.87 \pm 0.94	107.47 \pm 0.36	30.15 \pm 0.16
	average_time	20.53 \pm 1.41	0.03 \pm 0.01	0.47 \pm 0.12	0.44 \pm 0.06
<i>humanoid</i>	total_cost	194.57 \pm 46.90	18456.23 \pm 59.15	22606.60 \pm 70.25	790.85 \pm 58.81
	average_time	44.36 \pm 8.37	0.05 \pm 0.01	5.49 \pm 2.00	5.48 \pm 1.88

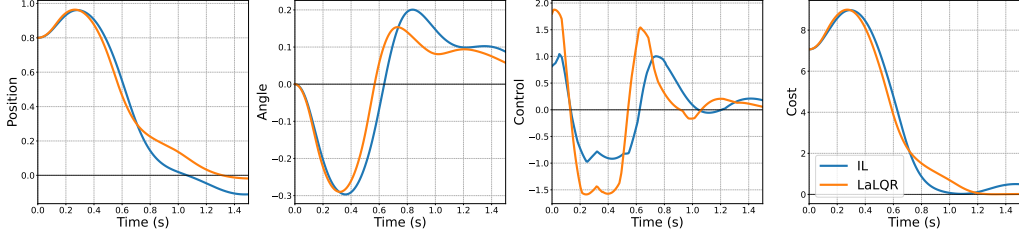


Figure 4: Control process of methods learned from imperfect experts. The x-axis is the real testing time, and the y-axis represents the partial state, control and cost in *cartpole* task.

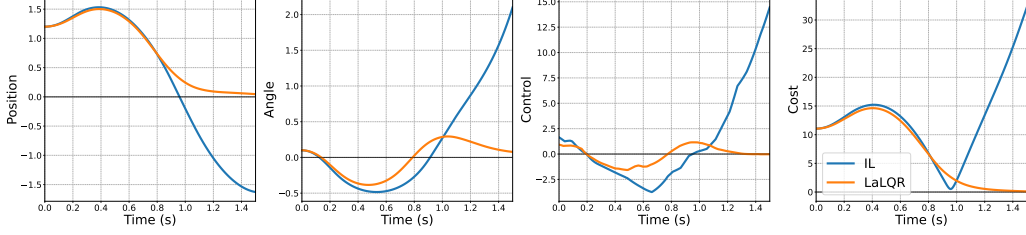


Figure 5: Control process of methods starting from unseen initial states in training. The x-axis is the real testing time, and the y-axis represents the partial state, control and cost in *cartpole* task.

4.3 Generalization

It is well-known that learning-based methods commonly suffer from the issue of generalization. They exhibit superior performances when the testing environment is the same as the training one, but quickly worsen even with slight mismatches. Here, we evaluate the generalization of two learning-based methods: IL and LaLQR in two specific scenarios: training with the imperfect expert and testing under the unseen initial state.

Imperfect Expert In the last section, we perform IL and LaLQR by imitating a well-performed SQP controller. In this section, we use an imperfect controller to sample trajectories and validate whether the learner can generalize to better control performance. In detail, with probability 0.5 at each step, we add a uniform noise $[-1, 1]$ on top of the controls generated by SQP. The other processes are kept the same as in the last experiment. Figure 4 indicates that IL controller is influenced by the added noise and generates sub-optimal controls (with cost > 0 in the end). In comparison, our method generalizes beyond the imperfect control data and still reaches zero position in the end.

Unseen Initial State In this experiment, we further test the generalization by initializing the state that is out of the training data. During the training in the *cartpole* task, all runs are started with the position from -1 to 1 and the angle equal to 0 . During testing, we set the position to 1.2 and the angle to 0.1 . As is shown in Figure 5, the IL controller completely fails at this initial stage, while LaLQR can maintain a stable performance. These two experiments strongly prove that imitating the whole MPC problem instead of the output alone can largely improve the generalization.

4.4 Ablation Study

In this section, we execute an ablation study on different designs of the proposed method. The first design is the structure of the linear dynamics matrix A . In Section 3.1, we mention besides companion form, there are also other forms such as diagonal matrix and full matrix. We compare these two forms in the *cartpole* task. As illustrated in Figure 6, in terms of the cost, the companion matrix (LaLQR) is the best, while the diagonal matrix is the worst. It corresponds to the theoretical analysis that the real-valued diagonal matrix can't fully represent the eigenvalues of the original nonlinear system despite its simplest structure. The full matrix has the same representation ability

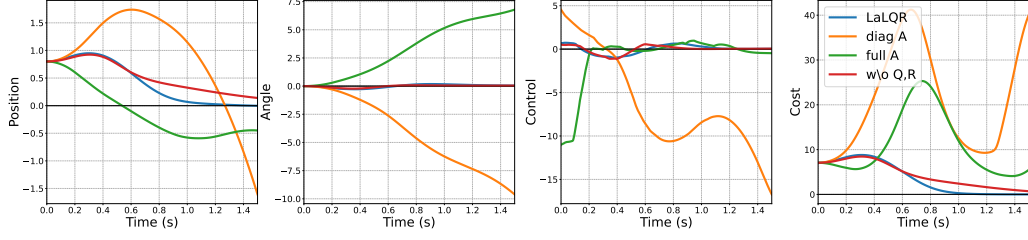


Figure 6: Control process of LaLQR with different design choices. The x-axis is the real testing time, and the y-axis represents the partial state, control and cost respectively in *cartpole* task.

as the companion matrix but is difficult to learn due to its larger parametric space. The second design that separates our method from previous related work is the cost loss in training the latent space. We remove this loss and only adopt the consistency loss to train the embedding function ϕ and the model dynamical model A , B , and fix Q , R as the identity matrix. The red curve in Figure 6 shows that it can still generate reasonable controls but react slower. Generally speaking, the model structure plays a more essential role in our proposed method and the cost function can improve the control performances by providing different weights to latent dimensions.

5 Related Work

Koopman operator has been increasingly popular in the robotics literature, thanks to its ability to transform the original state into the latent state, which can potentially assist the theoretical analysis and simplify downstream tasks. Extending dynamic mode decomposition (eDMD) [11, 17] is a standard numerical approach to finding the Koopman operator. The objective of eDMD is similar to consistency loss in our paper. The aim of these works is mainly to predict the future states instead of optimizing controls, which is distinguished from our work. Gadginmath et al. [18] adopted an equivalent companion structure on the latent dynamics. However, its control u is also mapped into a latent space v , making it difficult to recover the original control inputs, while this complex procedure can be omitted in our case. Mondal et al. [12] extended the previous work by also learning the cost function on the latent space. However, the cost function is still nonlinear and the complex-valued dynamics result in inefficient use.

Another parallel research branch in reinforcement learning is self-predictive learning [19, 20, 21]. These works are mainly motivated by learning an abstraction state from high-dimensional observation like images, which is opposite to our method. Besides, most of these works learn the latent space with auxiliary losses, e.g. the reconstruction loss to correctly predict future observations [19, 20], reinforcement learning loss to improve the policy [22, 23], which might be too complex and unnecessary for controls. Recently, more works have started to study the underlying principles of self-predictive learning. Tang et al. [14] proved the necessary condition to avoid representation collapse is that the dynamical model should be simpler than the embedding function, which is satisfied by a linear matrix and a nonlinear neural network in our cases. Ni et al. [24] claimed that using consistency loss and cost loss alone without reconstruction loss is enough to learn meaningful representation, which is also validated in our experiments.

6 Conclusion

In conclusion, the proposed latent linear quadratic regulator (LaLQR) method effectively addresses the computational challenges of model predictive control (MPC) in systems with nonlinear dynamics. Compared to other efficient solutions, LaLQR presents better control performances and enhanced generalization capabilities. This novel approach holds promise for advancing the practical application of MPC in embedded systems, which is crucial for real-time control in complex robotic environments. For future work, safety constraints should be considered in the latent system for

practical usage. Additionally, the incorporation of learnable modules can enable the use of domain randomization [25] techniques, enhancing the robustness and practicality of applying MPC to real-world robots. Finally, more advanced techniques [26] to solve linear control problems can be incorporated into our system for faster-embedded applications.

Acknowledgments

If a paper is accepted, the final camera-ready version will (and probably should) include acknowledgments. All acknowledgments go at the end of the paper, including thanks to reviewers who gave useful comments, to colleagues who contributed to the ideas, and to funding agencies and corporate sponsors that provided financial support.

References

- [1] J. Di Carlo, P. M. Wensing, B. Katz, G. Bledt, and S. Kim. Dynamic locomotion in the mit cheetah 3 through convex model-predictive control. In *2018 IEEE/RSJ International Conference on Intelligent Robots and Systems (IROS)*, pages 1–9, Madrid, Oct. 2018. IEEE. ISBN 978-1-5386-8094-0. doi:[10.1109/IROS.2018.8594448](https://doi.org/10.1109/IROS.2018.8594448).
- [2] R. Grandia, F. Jenelten, S. Yang, F. Farshidian, and M. Hutter. Perceptive locomotion through nonlinear model-predictive control. *IEEE Trans. Robotics*, 39(5):3402–3421, 2023. doi:[10.1109/TRO.2023.3275384](https://doi.org/10.1109/TRO.2023.3275384).
- [3] Y. Song and D. Scaramuzza. Learning high-level policies for model predictive control. In *2020 IEEE/RSJ International Conference on Intelligent Robots and Systems (IROS)*, pages 7629–7636, Oct. 2020. doi:[10.1109/IROS45743.2020.9340823](https://doi.org/10.1109/IROS45743.2020.9340823).
- [4] M. Diehl, H. J. Ferreau, and N. Haverbeke. Efficient numerical methods for nonlinear mpc and moving horizon estimation. In M. Morari, M. Thoma, L. Magni, D. M. Raimondo, and F. Allgöwer, editors, *Nonlinear Model Predictive Control*, volume 384, pages 391–417. Springer Berlin Heidelberg, Berlin, Heidelberg, 2009. ISBN 978-3-642-01093-4 978-3-642-01094-1.
- [5] J. Nocedal and S. J. Wright. Sequential quadratic programming. In *Numerical Optimization*, pages 526–573. Springer-Verlag, New York, 1999. ISBN 978-0-387-98793-4.
- [6] Y.-S. Wang, N. Matni, and J. C. Doyle. Localized lqr optimal control. In *53rd IEEE Conference on Decision and Control*, pages 1661–1668. IEEE, 2014.
- [7] B. D. Anderson and J. B. Moore. *Optimal Control: Linear Quadratic Methods*. Courier Corporation, 2007.
- [8] A. Brohan, N. Brown, J. Carbajal, Y. Chebotar, J. Dabis, C. Finn, K. Gopalakrishnan, K. Hausman, A. Herzog, J. Hsu, J. Ibarz, B. Ichter, A. Irpan, T. Jackson, S. Jesmonth, N. J. Joshi, R. Julian, D. Kalashnikov, Y. Kuang, I. Leal, K.-H. Lee, S. Levine, Y. Lu, U. Malla, D. Manjunath, I. Mordatch, O. Nachum, C. Parada, J. Peralta, E. Perez, K. Pertsch, J. Quiambao, K. Rao, M. Ryoo, G. Salazar, P. Sanketi, K. Sayed, J. Singh, S. Sontakke, A. Stone, C. Tan, H. Tran, V. Vanhoucke, S. Vega, Q. Vuong, F. Xia, T. Xiao, P. Xu, S. Xu, T. Yu, and B. Zitkovich. Rt-1: Robotics transformer for real-world control at scale, Dec. 2022.
- [9] M. Korda and I. Mezić. Linear predictors for nonlinear dynamical systems: Koopman operator meets model predictive control. *Automatica*, 93:149–160, 2018.
- [10] P. J. Antsaklis and A. N. Michel. *A Linear Systems Primer*. Springer Science & Business Media, 2007.
- [11] B. Lusch, J. N. Kutz, and S. L. Brunton. Deep learning for universal linear embeddings of nonlinear dynamics. *Nature Communications*, 9(1):4950, Nov. 2018. ISSN 2041-1723. doi:[10.1038/s41467-018-07210-0](https://doi.org/10.1038/s41467-018-07210-0).
- [12] A. K. Mondal, S. S. Panigrahi, S. Rajeswar, K. Siddiqi, and S. Ravanbakhsh. Efficient dynamics modeling in interactive environments with koopman theory. In *The Twelfth International Conference on Learning Representations*, 2024.

- [13] N. Nolte, O. Kitouni, and M. Williams. Expressive monotonic neural networks. In *The Eleventh International Conference on Learning Representations*, Sept. 2022.
- [14] Y. Tang, Z. D. Guo, P. H. Richemond, B. A. Pires, Y. Chandak, R. Munos, M. Rowland, M. G. Azar, C. L. Lan, C. Lyle, A. György, S. Thakoor, W. Dabney, B. Piot, D. Calandriello, and M. Valko. Understanding self-predictive learning for reinforcement learning. In *Proceedings of the 40th International Conference on Machine Learning*, pages 33632–33656. PMLR, July 2023.
- [15] E. Todorov, T. Erez, and Y. Tassa. Mujoco: A physics engine for model-based control. In *2012 IEEE/RSJ International Conference on Intelligent Robots and Systems*, pages 5026–5033, Vilamoura-Algarve, Portugal, Oct. 2012. IEEE. ISBN 978-1-4673-1736-8 978-1-4673-1737-5 978-1-4673-1735-1. doi:[10.1109/IROS.2012.6386109](https://doi.org/10.1109/IROS.2012.6386109).
- [16] Y. Tassa, T. Erez, and E. Todorov. Synthesis and stabilization of complex behaviors through on-line trajectory optimization. In *2012 IEEE/RSJ International Conference on Intelligent Robots and Systems*, pages 4906–4913, Oct. 2012. doi:[10.1109/IROS.2012.6386025](https://doi.org/10.1109/IROS.2012.6386025).
- [17] M. O. Williams, I. G. Kevrekidis, and C. W. Rowley. A data-driven approximation of the koopman operator: Extending dynamic mode decomposition. *Journal of Nonlinear Science*, 25(6):1307–1346, Dec. 2015. ISSN 0938-8974, 1432-1467. doi:[10.1007/s00332-015-9258-5](https://doi.org/10.1007/s00332-015-9258-5).
- [18] D. Gadginmath, V. Krishnan, and F. Pasqualetti. Data-driven feedback linearization using the koopman generator. *CoRR*, abs/2210.05046, 2022. doi:[10.48550/ARXIV.2210.05046](https://doi.org/10.48550/ARXIV.2210.05046).
- [19] M. Watter, J. Springenberg, J. Boedecker, and M. Riedmiller. Embed to control: A locally linear latent dynamics model for control from raw images. In *Advances in Neural Information Processing Systems*, volume 28. Curran Associates, Inc., 2015.
- [20] D. Hafner, T. Lillicrap, J. Ba, and M. Norouzi. Dream to control: Learning behaviors by latent imagination. *arXiv:1912.01603 [cs]*, Mar. 2020.
- [21] N. A. Hansen, H. Su, and X. Wang. Temporal difference learning for model predictive control. In *Proceedings of the 39th International Conference on Machine Learning*, pages 8387–8406. PMLR, June 2022.
- [22] H. Yin, M. C. Welle, and D. Kragic. Embedding koopman optimal control in robot policy learning. In *2022 IEEE/RSJ International Conference on Intelligent Robots and Systems (IROS)*, pages 13392–13399, Kyoto, Japan, Oct. 2022. IEEE. ISBN 978-1-66547-927-1. doi:[10.1109/IROS47612.2022.9981540](https://doi.org/10.1109/IROS47612.2022.9981540).
- [23] M. Retchin, B. Amos, S. Brunton, and S. Song. Koopman constrained policy optimization: A koopman operator theoretic method for differentiable optimal control in robotics. In *ICML 2023 Workshop on Differentiable Almost Everything: Differentiable Relaxations, Algorithms, Operators, and Simulators*, Sept. 2023.
- [24] T. Ni, B. Eysenbach, E. SeyedSalehi, M. Ma, C. Gehring, A. Mahajan, and P.-L. Bacon. Bridging state and history representations: Understanding self-predictive rl. In *The Twelfth International Conference on Learning Representations*, Oct. 2023.
- [25] X. B. Peng, M. Andrychowicz, W. Zaremba, and P. Abbeel. Sim-to-real transfer of robotic control with dynamics randomization. In *2018 IEEE International Conference on Robotics and Automation (ICRA)*, pages 3803–3810, May 2018. doi:[10.1109/ICRA.2018.8460528](https://doi.org/10.1109/ICRA.2018.8460528).
- [26] K. Nguyen, S. Schoedel, A. Alavilli, B. Plancher, and Z. Manchester. Tinympc: Model-predictive control on resource-constrained microcontrollers. In *IEEE International Conference on Robotics and Automation (ICRA)*, 2024.

- [27] T. Howell, N. Gileadi, S. Tunyasuvunakool, K. Zakka, T. Erez, and Y. Tassa. Predictive sampling: Real-time behaviour synthesis with mujoco, Dec. 2022.
- [28] I. Loshchilov and F. Hutter. Decoupled weight decay regularization. In *International Conference on Learning Representations*, Sept. 2018.

A Additional Algorithm Details

Algorithm 1 MPC Imitation Learning

- 1: **Input:** Nonlinear MPC’s dynamical model $f(x_h, u_h)$, cost function $c(x_h, u_h)$ and optimization algorithm to generate optimal control $u_h = \text{MPC}(x_h)$, initial state distribution $\Delta_{\mathcal{X}}$
 - 2: **Output:** Embedding function $z_h = \phi(x_h)$, gain matrix K
 - 3: Initialize dataset $\mathcal{D}_{\text{model}} = \{\}$
 - 4: **for** episode number $e = 1, 2, \dots, E$ **do**
 - 5: Sample an initial state $x_0 \sim \Delta_{\mathcal{X}}$
 - 6: **for** step $h = 0, 2, \dots, H$ **do**
 - 7: Generate optimal control u_h at state x_h with control rule $u_h = \text{MPC}(x_h)$
 - 8: Rollout for next state $x_{h+1} = f(x_h, u_h)$ and cost $c_h = c(x_h, u_h)$
 - 9: Store in the model dataset $\mathcal{D} \leftarrow \mathcal{D} \cup \{(x_h, u_h, c_h, x_{h+1})\}$
 - 10: **for** iteration $i = 1, 2, \dots, I$ **do**
 - 11: Sample B samples $(x_h^b, u_h^b, c_h^b, x_{h+1}^b)_{b=1}^B$ from the dataset \mathcal{D}
 - 12: Update parameters $p = (A, B, Q, R, F, \phi) = p - \lambda \nabla_p \sum_{b=1}^B \mathcal{L}_{\text{consistency}}(x_h^b, u_h^b, x_{h+1}^b) + \mathcal{L}_{\text{cost}}(x_h^b, u_h^b, c_h^b)$, where λ is the learning rate
-

B Additional Experimental Setups

B.1 Robotic Tasks on MuJoCo

We select 4 robots *cartpole*, *swimmer*, *walker* and *humanoid*, with increased complexity in state and action spaces as illustrated in Figure 3.

Cartpole *cartpole* has an un-actuated pole on top of a moving cart. In this task, the controller should balance the pole in the origin position. The state (4-dim) consists of the horizontal position and the angle from the vertical of the pole and their velocities. The control (1-dim) is the horizontal force on the cart. The cost is calculated as $c(x_t, u_t) = 0.1 \times c_{\text{velocity}}(x_t, u_t) + 0.1 \times c_{\text{control}}(x_t, u_t) + 10.0 \times c_{\text{centered}}(x_t, u_t) + 10.0 \times c_{\text{vertical}}(x_t, u_t)$. $c_{\text{velocity}}(x_t, u_t)$ is the absolute speed in horizontal direction. $c_{\text{control}}(x_t, u_t)$ is the norm of controls. $c_{\text{centered}}(x_t, u_t)$ is the absolute value of the position. $c_{\text{vertical}}(x_t, u_t)$ is the absolute value of the angle. The horizon is set to 1500.

Swimmer *swimmer* is a snake-like robot with 5 controllable actuators. In this task, the robot is driven to reach the target position. The state (16-dim) consists of the 3-D position of the robot, the positions of 5 actuators and their velocities. The control (5-dim) is the force of 5 actuators. The cost is calculated as $c(x_t, u_t) = 10.0 \times c_{\text{distance}}(x_t, u_t) + 0.1 \times c_{\text{control}}(x_t, u_t)$. $c_{\text{distance}}(x_t, u_t)$ is the distance from the target position. $c_{\text{control}}(x_t, u_t)$ is the norm of controls. The horizon is set to 500.

Walker *walker* is a bipedal robot with 3 controllable motors on each leg. In this task, the controller should balance the robot at a certain height. The state (18-dim) consists of the 3-D position of the robot, the positions of 6 actuators and their velocities. The control (6-dim) is the force of 6 motors. The cost is calculated as $c(x_t, u_t) = 1.0 \times c_{\text{velocity}}(x_t, u_t) + 0.1 \times c_{\text{control}}(x_t, u_t) + 10.0 \times c_{\text{height}}(x_t, u_t) + 3.0 \times c_{\text{rotation}}(x_t, u_t)$. $c_{\text{velocity}}(x_t, u_t)$ is the absolute speed. $c_{\text{control}}(x_t, u_t)$ is the norm of controls. $c_{\text{height}}(x_t, u_t)$ is the deviation from the target height. $c_{\text{rotation}}(x_t, u_t)$ is the rotation angle of the robot. The horizon is set to 400.

Humanoid *humanoid* is a humanoid robot with 21 controllable motors on each leg. In this task, the controller should balance the robot at a certain height. The state (55-dim) consists of the 3-D position, the 4-D quaternion of the robot, the positions of 21 actuators and their velocities. The control (21-dim) is the force of 21 motors. The cost is calculated as $c(x_t, u_t) = 10.0 \times c_{\text{velocity}}(x_t, u_t) + 0.025 \times c_{\text{control}}(x_t, u_t) + 100.0 \times c_{\text{height}}(x_t, u_t) + 3.0 \times c_{\text{balance}}(x_t, u_t)$. $c_{\text{velocity}}(x_t, u_t)$ is the absolute speed of centre of mass. $c_{\text{control}}(x_t, u_t)$ is the norm of controls.

$c_{\text{height}}(x_t, u_t)$ is the deviation from the target height. $c_{\text{balance}}(x_t, u_t)$ measures the relative position of the centre of mass between legs. The horizon is set to 400.

B.2 Hyperparameters of Baselines

We list the hyperparameters for all baselines in the paper.

SQP SQP requires prior knowledge of the nonlinear dynamical model f and cost function c , which can be directly achieved from the MuJoCo platform. The optimization is calculated based on iLQG [16], essentially a Gauss-Newton method utilizing first- and second-order derivative information. The detailed implementation follows the source code from Howell et al. [27]. The specific parameters for each task is set differently to adapt tasks, as illustrated in Table 3.

Table 3: Hyperparameters of SQP for all environments.

SQP Parameters	<i>cartpole</i>	<i>swimmer</i>	<i>walker</i>	<i>humanoid</i>
agent planner	1	2	2	0
agent timestep	0.01	0.01	0.01	0.015
agent horizon H	100	200	80	25

LoLQR LoLQR expands the nonlinear dynamical model at the stable point (x^*, u^*) with Taylor expansion, and uses the ground truth cost function c to calculate control laws. The stable point can be achieved by the final solution of SQP controller.

IL IL directly learns a control policy $u_h = \pi(x_h)$ by imitating the output of SQP with a neural network. The network structure is set as a 2-layer feed-forward neural network with $2N, N$ hidden units. The training dataset is created by rollouts in each environment with SQP controller for 200 episodes. The model is updated for 20 epochs with 128 batch size, and the optimizer is AdamW [28] with a learning rate of 0.001. The dimension N of the latent space for each task can be referred to Table 4.

LaLQR (Ours) Most hyperparameters and training datasets of LaLQR are set equally as IL for a fair comparison. The q embedding function is implemented as a neural network, with a one-layer feed-forward neural network with $2N$ hidden units. The output dimension is N so that the gain matrix K has the size $N \times m$, which has similar parameters as the policy network of IL. The model is updated for 20 epochs with 128 batch size, and the optimizer is AdamW [28] with a learning rate of 0.001. The dimension N of the latent space for each task can be referred to Table 4.

Table 4: Dimension of latent space of IL and LaLQR for all environments.

Parameters	<i>cartpole</i>	<i>swimmer</i>	<i>walker</i>	<i>humanoid</i>
hidden dimension N	20	50	60	210

B.3 Compute Resources

All experiments were performed on a server with 188GB of memory and an Intel Xeon(R) Silver(R) 4210 40-core CPU.

C Additional Experimental Results

C.1 Additional Training Results

We plot the training curves of LaLQR on all tasks in Figure 7. In general, this is not a difficult task for our proposed method as all losses gradually decrease to 0 in all tasks.

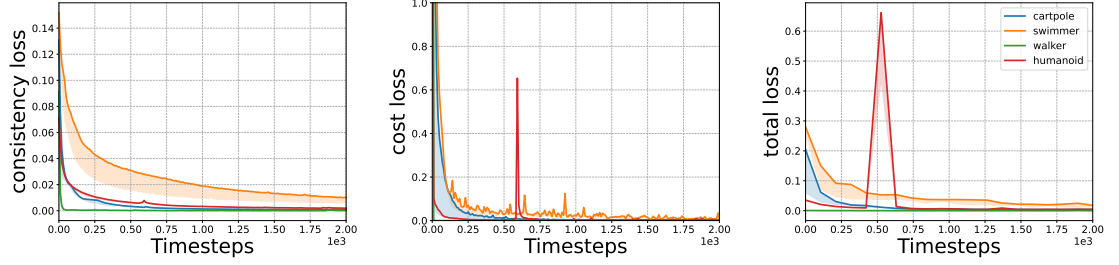


Figure 7: Training curves of LaLQR on all tasks. The a-xis is the training time steps, and the y-axis are training objectives of consistency loss, cost loss and total loss respectively. All results are plotted with the average and standard deviation shading over 5 random seeds